# Tet2-driven Clonal Hematopoiesis Drives Aortic Aneurysm via Macrophage-to-Osteoclast-like Differentiation

Jun Yonekawa[1,9], Yoshimitsu Yura[1,9*], Junmiao Luo[1], Katsuhiro Kato[1], Shuta Ikeda[2], Yohei Kawai[2,3], Tomoki Hattori[1], Ryotaro Okamoto[1], Mari Kizuki[1], Emiri Miura-Yura[4], Keita Horitani[5], Kyung-Duk Min[6], Takuo Emoto[7], Hiroshi Banno[2], Mikito Takefuji[1], Kenneth Walsh[8], Toyoaki Murohara[1]

[1]Department of Cardiology, Nagoya University Graduate School of Medicine, Nagoya, Japan
[2]Division of Vascular and Endovascular Surgery, Department of Surgery, Nagoya University Hospital, Nagoya, Japan
[3]Department of Vascular Surgery, Aichi Medical University, Nagakute, Japan.
[4]Division of Diabetes, Department of Internal Medicine, Aichi Medical University School of Medicine, Nagakute, Japan.
[5]Department of Medicine II, Kansai Medical University, Osaka, Japan
[6]Department of Cardiovascular and Renal Medicine, Hyogo Medical University, Hyogo, Japan.
[7]Division of Cardiovascular Medicine, Department of Internal Medicine, Kobe University Graduate School of Medicine, Kobe, Japan
[8]Division of Cardiovascular Medicine, Robert M. Berne Cardiovascular Research Center, University of Virginia School of Medicine, Charlottesville, VA, United States
[9]These authors contributed equally to this paper

**Short Title: Tet2-clonal hematopoiesis drives aortic aneurysm**

[*]**Corresponding Authors:**
Yoshimitsu Yura, MD, Ph.D.
ORCID: 0000-0003-2618-8569
Department of Cardiology
Nagoya University Graduate School of Medicine
Nagoya 466-8550, Japan
yura.yoshimitsu.z6@f.mail.nagoya-u.ac.jp
+81-52-744-2150

**Abstract**

Aortic aneurysms are age-linked aortic dilations that progress silently and carry high rupture mortality. Immune cells are recognized drivers of aneurysm pathogenesis. Clonal hematopoiesis is an age-related expansion of somatically mutated hematopoietic stem cells that reshapes immune function and contributes to diverse age-associated diseases. However, its contribution to aneurysm pathogenesis remains unclear. In this study, targeted ultradeep sequencing of patient specimens revealed a high prevalence of clonal hematopoiesis-associated mutations that correlated with faster aneurysm expansion. Thus, we modeled clonal hematopoiesis by competitively transplanting *Tet2*-deficient bone marrow into *Apoe*-knockout mice and induced aneurysms with angiotensin II. Tet2-clonal hematopoiesis mice developed significantly greater aortic dilation than controls. Interestingly, *Tet2*-deficient macrophages adopted an ACP5-positive, osteoclast-like state and produced more MMP9. Both genetic and pharmacological inhibition of osteoclast-like differentiation suppressed the Tet2-mediated aneurysmal growth in vivo. Thus, Tet2-driven clonal hematopoiesis accelerates aortic aneurysm progression through MMP9-producing osteoclast-like macrophages and therefore represents a tractable therapeutic axis.

**Brief Summary**

Clonal hematopoiesis accelerates aortic aneurysm growth by driving immune cells to become osteoclast-like and destructive, revealing a potential target for therapy.

## Introduction

Aortic aneurysms have emerged as a major age-related vascular disease that progresses silently and can lead to catastrophic rupture, for which surgical intervention remains the only effective treatment (1–3). Consequently, survival rates following rupture remain low, making aortic aneurysms a major cause of sudden death. While ischemic heart disease survival rates have increased since the 1980s due to advances in the treatment of hypertension, diabetes, and dyslipidemia, as well as improvements in cardiac catheterization (4), the outcomes for aortic aneurysms remain poor, underscoring their substantial unmet medical needs (5). Moreover, the lack of dependable clinical indicators beyond aneurysm diameter to predict disease progression remains a major barrier to effective long-term management of aortic aneurysms (6). Pathological features of aortic aneurysms include extracellular matrix degradation, loss of vascular smooth muscle cells, and inflammatory cell infiltration in the aortic wall (7–9). Calcification is also observed in aneurysms, as in atherosclerosis (10). However, features such as excessive matrix degradation and smooth muscle cell loss are more pronounced in aneurysms, highlighting the importance of analyzing disease-specific immune cell involvement to better understand the mechanisms underlying aortic aneurysm.

Clonal hematopoiesis has recently drawn attention for its link to age-related diseases (11, 12). It arises from somatic mutations in hematopoietic stem and progenitor cells, allowing mutant clones to expand in the bone marrow (13). This can occur subclinically in older adults, often involving mutations in epigenetic regulators such as Ten-eleven translocation 2 (TET2), DNA methyltransferase 3A (DNMT3A), and additional sex combs-like 1 (ASXL1), which disrupt normal hematopoiesis and immune function. As a result, immune cells derived from these mutant clones frequently adopt pro-inflammatory profiles, driving chronic inflammation implicated in multiple cardiovascular diseases (14, 15) , as well as osteoporosis, chronic obstructive pulmonary disease, and chronic liver disease (16–18). Despite the growing body of evidence linking clonal hematopoiesis to age-related diseases, its relationship with aortic aneurysms remains largely unexplored. Therefore, this study aims to investigate the impact of clonal hematopoiesis on the development and progression of aortic aneurysms through a genetic study in humans and an experimental study in mice.

## Results

### Mice with hematopoietic *Tet2* mutations exhibit augmented aortic dilatation following infusion of Angiotensin II (AngII)

To investigate the impact of clonal hematopoiesis on aortic aneurysm, we established a combined model of abdominal aortic aneurysm (AAA) and clonal hematopoiesis in mice. In human clonal hematopoiesis, a small fraction of mutant cells coexists with normal cells and gradually expands over time. To recapitulate this phenomenon in a mouse model, chimeric bone marrow was prepared by mixing 20% mutant cells with 80% normal cells and was transplanted into myeloablated Apolipoprotein E (*Apoe*)-deficient mice (Fig. 1 A), enabling the establishment of a clonal hematopoiesis model where mutant cells are initially present at a low proportion. The  gene was used as a representative model of clonal hematopoiesis because it is among the most biologically well-characterized clonal hematopoiesis drivers with established relevance to vascular inflammation (11). To distinguish  mutant from wild-type (WT) cells, different CD45 isoforms were used: mutant cells were labeled with CD45.2, while normal cells were labeled with CD45.1. The proportion of mutant cells was then evaluated through flow cytometric analysis of peripheral blood. Despite normal peripheral blood cell counts (Fig. 1 B), *Tet2* mutant cells exhibited a robust expansion in the peripheral blood (Fig. 1 C, D), consistent with the clinical paradigm of clonal hematopoiesis. At one-month post-bone marrow transplantation, echocardiographic assessment revealed no overt abnormalities in aortic structure, and there were no differences in aortic diameter or blood pressure between mice receiving control versus *Tet2*-mutant cells. These results indicate that, at baseline, mice harboring a substantial fraction of *Tet2*-mutant hematopoietic stem and progenitor cells (HSPCs) do not exhibit overt hematologic or vascular abnormalities.

The model described above was then subjected to Angiotensin II stimulation, a well-established method for inducing AAA (19). Both *Tet2*-mutant ($Tet2^{-/-}$) and WT ($Tet2^{+/+}$) groups exhibited comparable increases in systolic blood pressure (Fig. 1E). Nevertheless, echocardiographic analyses revealed a marked dilation of the abdominal aorta in the hematopoietic *Tet2*-mutant mice (Fig. 1F, G). Histological analysis confirmed thinning and fragmentation of elastic fibers in the vascular media of *Tet2*-mutated mice (Fig. 1

H, I). Collectively, these findings demonstrate that Tet2-driven clonal hematopoiesis accelerates aortic expansion, underscoring its pathogenic role in AAA.

**Detection of Clonal Hematopoiesis in Patients with Aortic Aneurysm**

To assess the clinical relevance of our findings, we analyzed peripheral blood samples from 44 patients with aortic aneurysm undergoing stent graft placement (Fig. 2A). Using error-corrected next-generation sequencing, we quantified clonal hematopoiesis-related mutations in DNA extracted from blood samples collected from these patients (20). Targeted analysis included 17 genes, including those involved in epigenetic regulation (DNMT3A, TET2, and ASXL1), DNA damage response pathways (tumor protein p53 [TP53], protein phosphatase, $Mg^{2+}$/$Mn^{2+}$ dependent 1D [PPM1D], ataxia telangiectasia mutated [ATM], and checkpoint kinase 2 [CHK2]), and RNA splicing (serine and arginine rich splicing factor 2 [SRSF2] and splicing factor 3b subunit 1 [SF3B1]). The full list is shown in Supplemental Table.1. The presence of these mutations and the proportion of mutated cells were quantified. As expected, we observed an increase in the proportion of individuals with clonal hematopoiesis in older group when dividing patients into three age groups (-74, 75-79, 80-90) (Fig. 2B). Collectively, we found that 60% of patients carried at least one gene mutation, and 35% harbored two or more (Fig. 2C). Notably, the overall frequency of clonal hematopoiesis-related mutations, particularly in DNMT3A and TET2 (Fig. 2D), was higher than the prevalence reported in population-based cohorts using non–error-corrected sequencing (21). The majority of the variant allele frequencies (VAFs) ranged from 0.5% to 2%, although larger clones exceeding 10% were also observed in some cases (Fig. 2E). In terms of mutation types, missense, frameshift, and stop codon gain mutations were observed at roughly equal frequencies (Fig. 2F). Numerous amino acid substitutions were identified and C>T substitutions in DNA were the most common (Fig. 2G).

Table 1 summarizes the baseline characteristics of the study population. When patients with clonal hematopoiesis were compared with those without clonal hematopoiesis, no statistically significant differences were observed in age (75.8 ± 6.5 vs 73.4 ± 8.7 years, P = 0.33), sex (male: 89.3 % vs 93.7 %, P = 0.63), BMI, eGFR, or the prevalence of hypertension, diabetes mellitus, dyslipidemia, coronary artery

disease, heart failure, smoking status, family history, or surgical method. Next, we retrospectively analyzed the expansion of aortic aneurysms in patients for whom longitudinal imaging was available. Table 2 shows the characteristics of this subgroup, which was comparable to the overall cohort in demographic and clinical characteristics. Follow-up duration was similar between the negative and positive clonal hematopoiesis groups (no-CH: 11.4 ± 2.6 months; CH: 11.3 ± 2.7 months, respectively). Representative CT scan images from patients with and without clonal hematopoiesis, taken one year before intervention and just prior to intervention, are shown (Fig. 2H). Strikingly, patients with clonal hematopoiesis exhibited significantly greater aortic aneurysm growth prior to requiring surgical intervention (4.3 ± 2.8 vs 2.8 ± 1.3 mm/year, P = 0.036) (Fig. 2I). We assessed whether clone size at surgery was associated with aneurysm progression and found no association between VAF and aneurysm growth rate in univariable linear regression analysis. These clinical data support our experimental findings and suggest that clonal hematopoiesis contributes to aortic aneurysm progression in humans.

**Bone marrow-derived macrophages play an essential role in aortic dilatation driven by Tet2 clonal hematopoiesis**

Somatic mutations that arise in hematopoietic stem cells are passed on to all multiple blood lineages. Thus, to clarify the culprit cell population in AAA progression in the mouse clonal hematopoiesis model, we infused AngII into *Apoe*-deficient mice and profiled aortic immune cells by flow cytometry one week later (Fig. 3A). Among the major leukocyte subsets, including monocytes, neutrophils, macrophages, T cells, and B cells, only macrophages were found to be significantly increased in the AngII condition relative to saline control, although there were non-significant trends toward increased numbers of neutrophils and Ly6C-high monocytes (Fig. 3B, C, and Fig. S1). We further distinguished yolk-sac-derived $CCR2^{-}$ macrophages from bone-marrow-derived $CCR2^{+}$ macrophages, revealing a selective expansion of the $CCR2^{+}$ subset (Fig. 3B, C). Collectively, these findings indicate that bone-marrow-derived macrophages may participate in the accelerated AAA development.

Immunostaining of aortic tissue in *Tet2*-mutant mice revealed that macrophages accumulate beneath the vascular endothelium, coinciding with abnormal smooth muscle cell proliferation in the aortic wall (Fig. 3D). To further investigate their role, macrophages were isolated from aorta using FACS sorting and subjected to RNA sequencing (Fig. 3E). This analysis identified 333 significantly upregulated genes and 154 downregulated genes (Fig. 3F, G, H) in the *Tet2* mutant condition. Among the differentially expressed genes, Acp5 [Tartrate-resistant acid phosphatase type 5 (TRAP)] was among those with the most significant q-values and represented an unexpected finding. Given prior reports implicating TRAP-positive macrophages in aneurysm pathology (22), we focused subsequent analyses on TRAP during osteoclast-like cell differentiation. TRAP-positive macrophages are known to secrete matrix metalloproteinase 9 (MMP9), an enzyme that degrades elastic fibers and contributes to aneurysm progression (22). Consistent with the RNA sequence data from aortic cells, cultured *Tet2*-mutant bone marrow derived macrophages exhibited an increased propensity to differentiate into TRAP-positive cells and showed elevated MMP9 mRNA expression (Fig. 3I, J, K). Therefore, we hypothesized that the underlying mechanism could involve the propensity of *Tet2*-mutant macrophages to differentiate into TRAP-positive macrophages, leading to MMP9 production and the destruction of elastic fibers that contribute to aortic aneurysm expansion.

**Receptor activator of nuclear factor κB (RANK)-RANK Ligand (RANKL) pathway has critical role in the TRAP positive macrophage differentiation and AAA disease progression in mice with Tet2 clonal hematopoiesis**

To directly test the role of TRAP-positive cells in Tet2-mediated acceleration of AAA, we disrupted the RANK-RANKL pathway, which plays a key role in promoting macrophage differentiation into osteoclast-like, TRAP-positive cells (23, 24). RANK is a type I transmembrane receptor composed of an extracellular domain containing multiple cysteine-rich TNF receptor-like motifs, a stalk region, a transmembrane domain, and a cytoplasmic tail that recruits adaptor proteins such as TRAF6 to activate downstream pathways including NF-κB (23, 25). To achieve a functional knockout (KO) of RANK, we used a CRISPR-Cas9 strategy targeting the cytoplasmic domain of mouse *Rank* and introduced a frameshift

mutation predicted to disrupt downstream signaling. Bone marrow cells were harvested from *Tet2*$^{+/-}$Cas9-expressing mice, enriched for hematopoietic stem cells by removing lineage positive cells, and infected with lentiviruses expressing mouse *Rank*-targeting gRNA and the reporter protein RFP to induce CRISPR-Cas9-mediated gene editing prior to transplantation (Fig. 4A). One month after BMT, we collected peripheral blood and performed flow cytometry. This analysis revealed that approximately 90% of CD45-positive cells were RFP-positive, indicating successful lentivirus infection (Fig. 4B, C). Additionally, insertion and deletion (Indel) mutations were observed in 70% of the CD45 cells, verifying efficient gene editing (Fig. 4D). Western blot analysis using a RANK antibody recognizing the N-terminal extracellular domain confirmed the loss of RANK protein in edited cells (Fig. 4E). Importantly, these mice with the edited *Rank* gene exhibited no overt abnormalities in peripheral blood cell counts (Fig. 4F). Using bone marrow cells from these mice, an in vitro osteoclast differentiation assay demonstrated that RANK-deficiency significantly suppressed macrophage differentiation into TRAP-positive cells after RANKL treatment (Fig. 4G, H). We next administered Ang II to evaluate aortic dilation in the clonal hematopoiesis/AAA model. Compared to *Tet2*-mutant/*Rank*-wild-type mice, mice transplanted with *Tet2*/*Rank* double-mutant bone marrow exhibited significantly greater reductions in aortic aneurysm expansion, thicker elastin fibers and less fiber rupture (Fig. 4I, J, K, L). Collectively, these findings demonstrate that RANK-deficiency suppresses macrophage differentiation into osteoclast-like TRAP-positive cells and ameliorates the aortic aneurysms observed in the Tet2 clonal hematopoiesis models, underscoring the critical role of this pathway in disease progression.

**Pharmacological inhibition of macrophage differentiation into TRAP-positive cells ameliorates AAA in mice with Tet2 clonal hematopoiesis.**

To corroborate these genetic findings, we investigated the efficacy of a pharmacological inhibitor targeting osteoclasts. Bisphosphonates, such as alendronate, inhibit the mevalonate pathway in osteoclast precursors by blocking the prenylation of small GTPase proteins (26). Through this mechanism, alendronate prevents the differentiation of macrophages into TRAP-positive osteoclast-like cells. Thus, cell culture

experiments were performed to test whether this drug could suppress the differentiation of *Tet2*-mutant macrophages into TRAP-positive osteoclast-like cells. *Tet2*-mutant macrophages, which exhibit an increased propensity for osteoclast-like differentiation, were significantly inhibited in their differentiation into TRAP-positive cells upon treatment with alendronate (Fig.5A, B). To evaluate whether pharmacological inhibition of this pathway could ameliorate the aortic aneurysm phenotype, the mouse AAA model was also treated with alendronate via subcutaneous injection (Fig.5C). Alendronate significantly ameliorated the phenotype in the angiotensin-induced AAA model, and the differences between the WT and Tet2 groups were no longer statistically significant (Fig. 5D, E, F, G). In addition to the subcutaneous injection, oral alendronate was administered daily by gavage after a 4-hour fast, with food withheld for 30 minutes post-dose, beginning on Day 0 of AngII infusion (Sup Fig 3A). Similar to the subcutaneous treatment, oral alendronate significantly suppressed aortic aneurysm expansion, and the difference between *Tet2*-mutant and WT groups was no longer detectable (Sup Fig 3B, C, D, E), indicating that the more clinically relevant route of oral alendronate administration is also effective in attenuating aneurysm progression.

Finally, a separate cohort of mice received an anti-RANKL monoclonal antibody, that prevents osteoclast-like differentiation of macrophages (27, 28), once every two days (Fig. 6A). As expected, the control IgG had no effect on aneurysm formation as the *Tet2*-mutant group treated with control IgG exhibited accelerated aneurysm expansion (Fig 6B, C), consistent with initial experiments (Figure 1F, G). Strikingly, anti-RANKL treatment significantly reduced aortic diameter compared with IgG-treated controls in both WT and *Tet2*-mutant group, and the difference between genotypes became undetectable (Fig. 6B, C, D, E). Collectively, these findings further support a causal role for RANK–RANKL–TRAP–mediated macrophage differentiation in promoting extracellular matrix degradation in *Tet2*-mutant conditions.

## Discussion

Aortic aneurysm is a life-threatening vascular condition that often progresses silently and can result in fatal rupture (1). Despite recognition of classical cardiovascular risk factors such as hypertension and dyslipidemia in aortic aneurysm pathogenesis, current pharmacological interventions targeting these factors have had limited efficacy in preventing aneurysm progression (5). Furthermore, no biomarkers have been identified that stratify patients by risk of aneurysm progression (6). These features highlight the unmet medical need in aortic aneurysm management and suggest that previously unrecognized mechanisms contribute to its pathology.

Studies have implicated various immune cells as key mediators of aortic aneurysm pathogenesis (7). Clonal hematopoiesis, a condition characterized by the age-related expansion of hematopoietic stem cells carrying somatic mutations, has emerged as a novel contributor to age-associated diseases by altering immune cell function (11). We therefore hypothesized that clonal hematopoiesis accelerates aortic aneurysm progression and set out to test this hypothesis experimentally and clinically. To determine whether clonal hematopoiesis is associated with aortic aneurysm progression in humans, we performed ultra-deep, error-corrected sequencing of blood samples from patients undergoing surgical repair for aortic aneurysms. We observed a high prevalence of mutations in clonal hematopoiesis-related genes, including TET2 and DNMT3A. Notably, patients with detectable clonal hematopoiesis exhibited more rapid aneurysm expansion prior to intervention, supporting a potential clinical link between these conditions.

Among known clonal hematopoiesis driver mutations, TET2 is of particular interest due to its known effects on myeloid cell activation and cytokine production (20, 29–31). To test whether Tet2 clonal hematopoiesis can affect aortic aneurysm in experimental system, we established a competitive bone marrow transplantation model in *Apoe*-knockout mice using bone marrow cells that displayed the expansion of the mutant hematopoietic cells. Upon AngII infusion, hematopoietic *Tet2*-mutant mice developed significantly larger aortic aneurysms compared with controls, along with marked elastin degradation and macrophage infiltration. Taken together, these mouse and human data identify clonal hematopoiesis as a previously unrecognized candidate accelerator of aortic aneurysm, with *Tet2* mutations mechanistically validated in a mouse model. Furthermore, flow cytometry and transcriptomic analyses revealed the selective

expansion of CCR2$^{+}$ *Tet2*-mutant macrophages with features suggestive of osteoclast-like differentiation. These findings raised the possibility that the *Tet2* mutation alters myeloid cell fate and contributes to aneurysm progression.

Mechanistically, we found that *Tet2*-deficient macrophages in the aortic wall display transcriptional signatures indicative of osteoclast differentiation. RNA sequencing of FACS-sorted macrophages revealed elevated expression of Acp5 (encoding TRAP), Ctsk (cathepsin K), and other genes associated with bone resorption, suggesting that hematopoietic *Tet2*-deficiency promotes the differentiation of macrophage to osteoclast-like cells. This phenotype was further confirmed in vitro, where *Tet2*-mutant bone marrow-derived macrophages exhibited enhanced RANKL-induced differentiation into TRAP-positive, multinucleated osteoclast-like cells. *Tet2*-deficient macrophages have been shown to upregulate inflammatory gene expression and produce large amounts of interleukins following stimulation (29, 32, 33). It is also known that differentiation of macrophages into osteoclast-like cells is promoted by inflammatory conditions (34, 35). These cells also secrete higher levels of MMP9, an enzyme known to degrade extracellular matrix components and weaken the aortic wall (36–38). Thus, to validate the functional relevance of this pathway, we genetically ablated RANK or pharmacologically inhibited osteoclast function using bisphosphonates or an anti-RANKL antibody. Both approaches significantly attenuated aneurysm formation such that the differences in aneurysm expansion between *Tet2*-mutant and WT conditions were no longer detectable. Taken together, these findings demonstrate that Tet2-driven clonal hematopoiesis promotes AAA progression by redirecting macrophage differentiation toward a tissue-destructive, osteoclast-like fate, thereby providing a mechanistic link between somatic mutations in hematopoietic cells and vascular degeneration. These findings provide a rationale for future clinical investigations. Although large-scale clinical studies examining bisphosphonate therapy are lacking, future studies could explore whether targeting RANK–RANKL can ameliorate aneurysm progression driven by some forms of clonal hematopoiesis.

Collectively we show that clonal hematopoiesis is prevalent among patients with aortic aneurysm and that carriers undergo significantly more rapid aneurysm expansion. Peripheral-blood clonal hematopoiesis screening could therefore serve as a minimally invasive biomarker, identifying high-risk individuals who merit closer imaging surveillance of aortic dilation. Beyond risk stratification, the mechanistic link between clonal hematopoiesis and aortic aneurysm shown here suggests tractable therapeutic avenues. The bisphosphonate alendronate and anti-RANKL antibody, which are typically used to treat bone diseases by inhibiting osteoclast differentiation and activity, were found to be effective in attenuating aortic aneurysm progression in the animal model. Because this anti-resorptive agent is approved for osteoporosis, the repurposing of these drugs for treating aortic dilation in clonal hematopoiesis-positive patients could enable, mutation-guided therapy for this otherwise intractable disease. Intriguingly, Dnmt3a-mediated clonal hematopoiesis has also been shown to exacerbate osteoporosis by activating osteoclast (18), which aligns with our current findings.

**Limitations**

While our study provides important insights into the role of Tet2-driven clonal hematopoiesis in aortic aneurysms, several limitations should be acknowledged. First, while we documented the role of macrophages, we cannot rule out the potential contribution of other immune cell subsets. Second, although we delineated a RANK-RANKL-dependent, osteoclast-like program as a key pathogenic axis, *Tet2*-mutant macrophages also release pro-inflammatory cytokines that may act in parallel or synergistically. This possibility can be addressed by future analyses. Third, the human study relies on a relatively small, single-ethnicity cohort and an observational design, limiting statistical power. Nonetheless, our use of high-fidelity, error-corrected next-generation sequencing enabled more sensitive detection of clonal hematopoiesis mutations than conventional biobank studies, and murine loss-of-function experiments provide causal evidence of the pathogenic potential of clonal hematopoiesis. Fourth, longitudinal imaging data for aneurysm growth were available only for a subset of patients, but this subgroup appeared broadly comparable to the overall cohort. Fifth, our cohort was limited to consecutive EVAR-treated patients;

therefore, the generalizability of our findings to patients undergoing open repair requires further study. Sixth, because clonal hematopoiesis was assessed at the time of surgery and longitudinal clonal hematopoiesis measurements were not available, we cannot fully exclude reverse causality. Finally, clonal hematopoiesis as a whole, but not individual mutations, was associated with accelerated aneurysm progression, likely reflecting relatively small sample size and genetic heterogeneity of individual driver mutations. However, mechanistic data from the Tet2 mouse model of clonal hematopoiesis indicates that this driver gene is causal for accelerated aneurysm expansion.

**Conclusions**

In summary, our data identify clonal hematopoiesis as a previously unrecognized contributor to aortic aneurysm progression. Mechanistic studies with *Tet2* gene reveal that clonal hematopoiesis promotes AAA progression via macrophage re-programming toward an osteoclast-like, matrix-degrading phenotype. Targeting the RANK–RANKL axis therefore represents a tractable precision-medicine strategy for this otherwise intractable disease.

## Materials and Methods

### Sex as a biological variable

This study examined male mice because male animals exhibited less variability in phenotype. It is unknown whether the findings are relevant for female mice.

This study included both male and female human subjects. The sex distribution is presented in Table 1. No sex-specific analyses were conducted, and the findings are considered to be broadly applicable across sexes.

### Clinical Data

This study was a retrospective observational cohort study. All participant data (including standard baseline demographics, laboratory data, and medical histories) were sourced from a Nagoya University cohort in Nagoya, Japan, and patients were included consecutively between December 2023 and February 2025. Race and ethnicity were self-reported, and all participants were Japanese. Blood samples for ultradeep error-corrected sequencing were collected at the time of surgical admission, and aneurysm growth rate prior to surgery was analyzed retrospectively. All patients were monitored with contrast-enhanced CT every 6–12 months according to standard clinical practice. All 44 patients included in this study had abdominal aortic aneurysms; thoracic aneurysms were not included. Longitudinal imaging data for aneurysm diameter were available in 21 of 44 patients. Patients with any clinical features suggestive of hereditary or syndromic aortopathies were excluded. Aortic diameter in the patient cohort was measured using contrast-enhanced CT, the standard modality for preoperative evaluation of abdominal aortic aneurysms. Maximum aneurysm diameter was determined by a board-certified radiologist who was blinded to clonal hematopoiesis status and clinical outcomes to ensure objective and unbiased assessment. Measurements were performed using axial and reconstructed sagittal images, and the largest cross-sectional diameter was recorded for analysis. This standardized approach was applied uniformly across all cases.

### Ultra-deep error-corrected DNA sequencing

Patient blood samples were collected at the time of surgical admission using PAXgene® DNA tubes (Cat# 761165, BD Biosciences) and cryopreserved until use. Ultra-deep error-corrected DNA sequencing was performed as previously described (20). Briefly, genomic DNA was isolated from the blood samples using QIAamp DNA extraction kits (Cat# 51104; Qiagen). The pooled libraries were sequenced using a NovaSeq X instrument (Illumina). Raw data from biological replicate error-corrected sequencing were analyzed as previously described (20). Briefly, a minimum of three raw reads sharing the same unique molecular identifier were used to generate an error-corrected consensus sequence. The output was filtered to include bases with ≥700× consensus read coverage within the target regions of a custom gene panel (Table S1), excluding common variants (minor allele fraction ≥0.01) identified by the 1000 Genomes Project (39). The selected gene panel incorporated well-documented clonal hematopoietic genes based on the IntoGen Clonal Hematopoiesis Mutation Browser database (40). For single-nucleotide variant calling, a position-specific binomial background error model was implemented for variant calling. Each genomic position was modeled independently by compiling the background error rate of normal samples for that specific genomic position, defined as the fraction of non-reference reads relative to the total number of sequencing reads at that position. For each individual sample, the number of reads supporting the non-reference allele at a given genomic position was compared with the corresponding background error rate. A genomic position was considered positive when the observed number of non-reference reads was significantly higher than the background error rate based on a binomial test ($P < 0.01$). Variants with VAF > 0.45 were removed to exclude potential germline variants, and those below this threshold occurring in three or more subjects were considered recurrent sequencing errors and omitted. Variants with VAF < 0.005 were excluded because of decreased confidence in distinguishing variants due to intrinsic sequencing error. Finally, only frameshift, stop-gain, and missense variants were included in the downstream analysis, as these mutations have the potential to influence protein function.

**Mice**

B6(Cg)-*Tet2*$^{tm1.2Rao}$/J (No: 023359), B6.129P2-*Apoe*$^{tm1Unc}$/J (No: 002052), C57BL/6J WT (No: 000664), and B6(C)-Gt(ROSA)26Sorem1.1(CAG-cas9*,-EGFP)Rsky/J (No: 028555) mice were obtained from Jackson Laboratories. B6.SJL-Ptprc$^{a}$ Pepc$^{b}$/BoyJ mice were obtained from Sankyo Labo Service Corporation.

**Cell culture**

For in vitro experiments, each biological replicate represents an independent culture derived from bone marrow cells obtained from different mice. A Lenti-X 293T cell line was obtained from Takara Bio. Cells were cultured in DMEM supplemented with 10% fetal bovine serum (FBS) and penicillin/streptomycin/L-glutamine (complete medium) at 37 °C in a humidified incubator with 5% $CO_2$. BM-derived macrophages were isolated and cultured in complete medium (RPMI 1640 supplemented with 10% FBS; Cat# 11-875-093 and Cat# SH3091003, respectively; Thermo Fisher Scientific). First, the bone marrow was flushed from the tibia and femurs of 8- to 10-week-old mice and cells were washed and cultured overnight in complete medium. Hematopoietic stem and progenitor cells were purified via differential plating and defined as the non-adherent population after 16 h of culture. Macrophage proliferation and differentiation were induced by culturing for 3 d in complete medium supplemented with macrophage colony-stimulating factor (M-CSF; 30 ng/mL; Cat# 315-02, PeproTech). Cells were then detached using 0.25% trypsin with EDTA (Cat# 25200056, Thermo Fisher Scientific) at 37 °C for 30 min to 1 h and reseeded in new plates containing M-CSF and RANKL (25 or 50 ng/mL; Cat# 315-11C, PeproTech). The cells were further incubated for 3 d in complete medium. To inhibit macrophage differentiation, alendronate sodium (0.5 μg/mL; Cat# A4978, Sigma-Aldrich) was added at the time of reseeding. Differentiation into osteoclast-like cells was assessed using a TRAP staining kit (Cat# AK04F; Cosmo Bio).

**Lentivirus production**

Plasmids pLKO5.sgRNA.EFS.tRFP (Cat# 57823), psPAX2 (Cat# 12260), and pMD2.G (Cat# 12259) were purchased from Addgene. A single-guide RNA (sgRNA) targeting exon 9 of the *Rank* gene was designed

using the CRISPR design tool (https://www.idtdna.com/site/order/designtool/index/CRISPR_CUSTOM). Single gRNA targeting mouse *Rank* (AGATTCTAGGACGTTCACAC) or a noncoding sgRNA targeting an intron in the murine *Actb* gene (aggttgctctgacaaccaca) were subcloned into the BsmB1 restriction enzyme site of the appropriate vector. Lentiviral particles were generated as previously described (41). Briefly, the plasmids (lentiviral vector, psPAX2, and pMD2.G) were co-transfected into Lenti-X 293T cells using polyethyleneimine. The culture supernatant was collected 48 h after transfection, filtered through a 0.45 μm filter, and concentrated by ultracentrifugation at 72 100 *g* for 3 h. The viral pellet was resuspended in StemSpan medium (Cat# 09600, STEMCELL Technologies) and stored at −80 °C. Lentiviral titers were determined using a Lenti-X qRT-PCR Titration Kit (Cat# 631235, Clontech).

**Isolation of lineage-negative bone marrow cells and lentivirus transduction**

Lineage-negative bone marrow cells were isolated using a lineage depletion kit (Cat# 130-090-858, Miltenyi Biotech) from mice generated by crossing B6(C)-Gt(ROSA)26Sorem1.1(CAG-cas9*,-EGFP)Rsky/J and B6(Cg)-*Tet2*<sup>tm1.2Rao</sup>/J, and selecting for heterozygous alleles of both strains. Cells were pre-incubated with StemSpan medium (Cat# 09600, STEMCELL Technologies) for 1.5 h at 37 °C. Lentivirus transduction was performed in 20 ng/mL thrombopoietin (Cat# 315-14, PeproTech), 50 ng/mL stem cell factor-1 (SCF-1; Cat# 250-03, PeproTech), and 4 μg/mL polybrene (Cat# 12996-81, Nacalai Tesque) for 16–20 h. The cells were collected and resuspended in RPMI medium before transplantation.

**Bone marrow transplantation**

Recipient mice were exposed to two radiation doses of 4.5 Gy at 4 h intervals using MBR-1618R-BE (Hitachi). For mouse models of clonal hematopoiesis, bone marrow cells containing 20% *Tet2*-KO and 80% WT cells ($5 \times 10^6$ cells in 200 μL RPMI 1640 medium/mouse) were retro-orbitally injected into 8- to 10-week-old *Apoe*-KO mice. For RNA-seq experiments, 100% *Tet2*-KO or 100% WT donor bone marrow was used. To distinguish between donor *Tet2*-KO and WT cells, WT cells were obtained from mice carrying

the CD45.1 variant of the CD45 hematopoietic antigen, whereas *Tet2*-KO cells were obtained from mice carrying the CD45.2 variant. Control mice (20% WT BMT) were transplanted with 20% CD45.2+ and 80% CD45.1+ WT cells. For lineage-negative cell transplantation, lentivirus-transduced cells ($5 \times 10^5$ cells in 200 μL RPMI 1640 medium/mouse) were used instead. The experimental mice were randomly assigned to either the experimental or control group. We did not exclude any mice with the exception of those that were not used due to human error. Although no power analyses were performed to determine sample sizes, appropriate sample sizes for statistical analysis were selected based on our previous experimental findings using the same models.

**qRT-PCR**

Total RNA from tissues and cultured cells was isolated using QIAzol reagent (Cat# 79306, Qiagen) and a NucleoSpin RNA Plus kit (Cat# 740984.50, Takara). RNA (0.5–1.2 μg) was reverse transcribed with a QuantiTect Reverse Transcription Kit (Cat# 205313, Qiagen). qRT-PCR was performed with Power SYBR® Green reagent (Cat# 4368708, Thermo Fisher Scientific) on a ViiA7 PCR system. A standard thermocycling protocol (95 °C for 15 s and 60 °C for 60 s, total 40 cycles) was used for gene amplification. Primer sequences included 5′-GCTCCAAGCAGATGCAGCA-3′ and 5′-CCGGATGTGAGGCAGCAG-3′ (*36b4*), 5′-GCGACCATTGTTAGCCACATACG-3′ and 5′-CGTTGATGTCGCACAGAGGGAT-3′ (*Trap*), and 5′-CTGGACAGCCAGACACTAAAG-3′ and 5′-CTCGCGGCAAGTCTTCAGAG-3′ (*Mmp9*). Gene expression was analyzed using the ΔΔCt method and normalized according to that of the reference gene *36b4*.

**Hematopoietic cell and flow cytometric analyses of peripheral blood and aortic immune cells**

Hematopoietic parameters were analyzed using a VETSCAN HM5 (Zoetis). Flow cytometric analysis of peripheral blood leukocytes and aortic immune cells was performed at the indicated time points as previously described (41). Peripheral blood cells were obtained from the retro-orbital vein and collected in

K2 EDTA-containing Fuji tubes (Cat# A01032, Fujifilm). Red blood cells were lysed in eBioscience 1X RBC Lysis Buffer (Cat# 00-4333-57, Thermo Fisher Scientific) for 5 min on ice. Incubation with antibodies was performed for 20 min at room temperature in the dark. Aorta tissues were minced and digested in collagenase I (450 U/mL), collagenase XI (125 U/mL), hyaluronidase (450 U/mL), and DNase I (60 U/mL) (Cat# C0130, C7657, H3506, and D4513, respectively, MilliporeSigma) at 37 °C for 30 min using a ThermoMixer C (Eppendorf) at 900 rpm. Aorta samples were subsequently homogenized using cell strainers (Falcon, Cat# 352350, Thermo Fisher Scientific). After incubation with antibodies, dead cells were excluded from the analysis using Zombie Aqua or Violet (Cat# 423102 and Cat# 423113, respectively; BioLegend) according to the manufacturer's instructions. To determine the cell numbers, 123count eBeads (Cat# 01-1234-42, Thermo Fisher Scientific) were used. Data acquisition was performed using Fortessa and analyzed using FlowJo software (FlowJo), and cell numbers were normalized to the number of cells/100 mg wet weight of the aorta. Flow cytometric analyses were performed using distinct antibody panels according to sample type and immune-cell subsets, as detailed in Supplemental table 2. The cells were defined as described in the gating strategy shown in Fig. S2.

**Echocardiographic analyses**

Echocardiography was performed on isoflurane-anesthetized mice. Mice were kept semi-awake in a shallow state of anesthesia by monitoring their responses to physical stimuli (tail pinch, etc.), and heart rate was maintained at 500–600 bpm. M-mode images of the abdominal aorta in the supraceliac region just above the bifurcation of the celiac artery were obtained using a Vevo 3100 imaging system (FUJIFILM VisualSonics) equipped with an MS400 (18-38 MHz) phased-array transducer.

Aortic diameter was assessed using high-resolution M-mode echocardiography at a standardized anatomical location immediately distal to the celiac arteries (42). The celiac artery was first identified in the long-axis view and centered on the screen, after which the probe was rotated 90° to obtain a consistent short-axis view. M-mode tracings were acquired at the site demonstrating the maximal vessel diameter. Measurements were performed at end-systole across three consecutive cardiac cycles. Aortic diameter was

defined as the distance from the midpoint of one medial layer to the midpoint of the opposite medial layer, ensuring consistent depth and perpendicular orientation across animals.

**Pump implantation**

To induce aortic aneurysms in mice, osmotic minipumps (Alzet model 2004; Cupertino, CA) containing either AngII (1.44 mg/kg/d, diluted in sterile saline, Cat# A9525, Sigma-Aldrich) or saline (sham) were implanted subcutaneously into a small pocket made through an incision at the nape of the neck. The mice were anesthetized with isoflurane during the entire surgical procedure, and the wounds were closed with wound clips. Osmotic minipumps were primed in PBS at 37 °C for 24 h before implantation, and they remained in place for 28 d post-implantation. In some experiments, the mice were implanted with a second minipump to prolong the time course. Blood pressure was measured using tail-cuff plethysmography, as previously described(41).

**Alendronate treatment**

For the bisphosphonate experiment, mice were subcutaneously injected twice per week with alendronate sodium (Cat# A4978, Sigma-Aldrich) at 100 μg/kg. Oral alendronate (1.4 mg/kg daily) was administered by gavage after a 4-hour fast, with food withheld for 30 minutes post-dose, beginning on Day 0 of AngII infusion.

**RANKL-blocking interventions in mice.**

Anti-RANKL monoclonal antibody (InVivoMAb anti-mouse RANKL, clone IK22/5; BE0191) was administered intraperitoneally at 4mg/kg per injection, once every two days. A rat IgG2a isotype control antibody (InVivoMAb, clone 2A3; BE0089) was used as the control.

**Histology**

Aorta tissues were perfused with cold PBS from the transected end and fixed in 10% formalin at 4 °C overnight. Samples were processed for paraffin embedding and cut into 4-μm-thick sections. For tissue staining, the sections were deparaffinized and rehydrated. To determine elastic fibers, aortic sections were stained with a Microscopy Elastica van Gieson staining kit (Cat# 1.15974.0002, Sigma-Aldrich). The images acquired using a BZ-X710 Keyence microscope were analyzed using ImageJ software (National Institutes of Health, Bethesda, MD) to quantify the elastic fiber thickness and number of tears. Elastin quantification: Elastin fiber thickness and elastin rupture were quantified in EVG-stained abdominal aortic sections. One section per mouse was analyzed, corresponding to the maximally dilated aneurysmal segment. Five non-overlapping high-power fields were selected per section in a blinded manner. Elastin thickness was measured at three predefined points per field along the medial elastic lamellae and averaged to obtain a single value per mouse. Elastin rupture was semi-quantitatively scored based on the percentage of disrupted elastic lamellae in each field, and the mean score across five fields was used for analysis. All measurements were performed by two independent investigators blinded to genotype and treatment group. $TRAP^+$ cell quantification: Five non-overlapping high-power fields per well were analyzed, and $TRAP^+$ cells were manually counted by two independent observers blinded to genotype and treatment group. Counts were averaged across fields to obtain a single value per well.

**Western blotting**

Bone marrow-derived macrophages were lysed directly in culture dishes using SDS sample buffer (Blue Loading Buffer, Cat# B7703S, New England BioLabs) containing 40 mM DTT, followed by incubation at 95 °C for 5 minutes. Cell lysates were separated using SDS-PAGE (Cat# 4561033, Bio-Rad Laboratories) and transferred to PVDF membrane. After blocking with 5% skim milk in PBS with Tween 20 (0.1%) for 1 h, the membranes were incubated with the indicated antibodies overnight at 4 °C, followed by HRP-conjugated second antibody (Cat# sc-2357, Santa Cruz Biotechnology) for 1 h at room temperature. The following antibodies were used for immunoblotting: β-Actin (13E5) rabbit monoclonal antibody (Cat# 4970, Cell Signaling Technology) and anti-RANK (EPR26196-15) rabbit monoclonal antibody (Cat# ab305233,

Abcam). Images were visualized using an ECL Prime Western Blotting System (Cat# RPN2232, GE Healthcare).

**Immunostaining**

For Smooth muscle actin, CD68, and platelet endothelial cell adhesion molecule-1 (PECAM-1) staining, aortic tissue sections were deparaffinized, and antigen retrieval was performed using Epitope Retrieval Solution pH 6 (Cat# RE7113-CE, Leica Biosystems). Sections were blocked with Protein Block Serum-Free (Cat# X0909, Agilent Technologies) for 30 min and subsequently incubated with primary antibody overnight at 4 °C. To distinguish target staining from the background, a secondary antibody was used as a negative control in each experiment. After washing with Tris-buffered saline, sections were incubated with secondary antibodies for 2 h at room temperature. Nuclei were stained with DAPI. Fluorescence images were captured using the BZ-X710 Keyence microscope. The primary antibodies included mouse anti-actin a-Smooth Muscle-Cy3 (1A4) (Cat# C6198, Sigma-Aldrich), rabbit CD68(E307V) (Cat# 97778, Cell Signaling Technology), and goat CD31/PECAM-1 (Cat# AF3628, R&D Systems). The secondary antibodies included donkey anti-rabbit Alexa488 (Cat# A21206, Thermo Fisher Scientific) and donkey anti-goat Alex647 (Cat# A21447, Thermo Fisher Scientific).

**Cell sorting**

For qPCR analysis of aorta macrophages ($CD45^{+}Ly6G^{-}CD64^{+}Ly6C^{-}$), aorta digests were prepared as described for the flow cytometric analysis and sorting was performed on a FACSAria Fusion cell sorter (BD Biosciences) with a 100 μM nozzle and flow pressure set to 20 psi. A total of 20,000 cells were sorted for each population.

**RNA sequencing**

Total RNA was extracted from the FACS-sorted aortic macrophages using an RNeasy Micro Kit (Qiagen). RNA integrity and concentration were assessed using a bioanalyzer (Agilent Technologies). RNA-seq

library preparation was outsourced to Takara Bio Inc.. Libraries were prepared using a SMART-Seq v4 Ultra Low Input RNA Kit combined with a Nextera XT DNA Library Prep Kit optimized for low-input polyA+ RNA. Sequencing was performed using an Illumina NovaSeq platform, which generated approximately 40 million paired-end reads per sample. The mouse GRCm39 (mm39) construct was used as the reference genome for alignment. Sequencing data, including read alignment, quantification, and expression of known transcripts, were processed using Expression Miner 2.0 (Takara Bio). For further downstream analysis, read count data were imported into R (v4.2.2) and differential expression analysis was conducted using the DESeq2 package. Genes with an adjusted $P < 0.05$ and |log2 fold change| > 1 were considered differentially expressed. Functional enrichment analyses (GO and KEGG) were performed using clusterProfiler, and Gene Set Enrichment Analysis was carried out using the fgsea and MSigDB hallmark gene sets.

**Statistical analysis**

For experimental (in vivo and in vitro) studies, all statistical analyses were performed using GraphPad Prism 10 (GraphPad Software). Data are presented as mean ± standard error of the mean (SEM). Data distribution was assessed using the Shapiro-Wilk normality test. For normally distributed data with one experimental variable, statistical analyses were performed using parametric tests: unpaired (two-tailed) Student's t-test for two groups with equal variance, or Welch's t-test for two groups with unequal variance, and one-way ANOVA with Tukey's multiple-comparison test for >2 groups. Data with two independent variables were evaluated using two-way ANOVA or two-way repeated measures ANOVA, as appropriate, followed by Sidak multiple-comparison post-hoc tests. For non-normally distributed data with one experimental variable, statistical analyses were performed using nonparametric tests: the Mann-Whitney *U* (two-tailed) test for two groups and Kruskal-Wallis with Dunn multiple comparison post-hoc tests for >2 groups. Statistical significance was set at $P < 0.05$. Statistical analyses were performed using biological replicates as independent samples. Statistical significance is shown only for selected pairwise comparisons relevant to the hypothesis.

For analyses of human clinical samples, continuous variables were summarized as mean ± standard deviation, and categorical variables as number (%). Between-group differences were assessed using Student's t-test or the Mann–Whitney U test for continuous variables and Pearson's chi-square test or Fisher's exact test for categorical variables, as appropriate. The association between CH status and aneurysm growth rate was evaluated using univariable linear regression. All P-values were two-sided, and a value of $P < 0.05$ was considered statistically significant. Statistical analyses were performed using GraphPad Prism 10 (GraphPad Software).

**Study approval**

The study protocols were approved by the Institutional Animal Care and Use Committee (IACUC) of Nagoya University (approval no. M250302-002). The study investigating the association between clonal hematopoiesis and abdominal aortic aneurysm was registered in the UMIN Clinical Trials Registry (UMIN000052118). Written informed consent was obtained from all participants prior to inclusion in the study.

**Data availability**

Supporting data values for all graphs and values underlying the reported means are provided in the Supporting Data Values file. All raw and processed RNA-sequencing data generated in this study have been deposited in the DDBJ Sequence Read Archive (DRA) under accession number DRP016820 (BioProject: PRJDB39638). Supporting numerical data underlying the graphs are provided in the Supplemental Data. Additional datasets used in this study are available from the corresponding author upon reasonable request. Clinical genomic data derived from human samples have been deposited in the NBDC Human Database under controlled access (accession number Study: JGAS000864 Dataset: JGAD001007). Access to these data requires approval from the NBDC Data Access Committee in accordance with institutional and national guidelines.

**Supplemental Materials**

Figures S1 to S3

Tables S1 and S2

**Acknowledgements**

The authors wish to acknowledge Division for Medical Research Engineering, Nagoya University Graduate School of Medicine.

**Funding**

This work was supported by the Japan Society for the Promotion of Science KAKENHI (grant 22K16136 and 24K19026), the Japan Science and Technology Agency (JST) FOREST (Fusion Oriented Research for Disruptive Science and Technology) Program (grant JPMJFR2217), the Japan Agency for Medical Research and Development (AMED) (grant JP256f0137010), the Japan Foundation for Applied Enzymology, Kowa Life Science Foundation, MSD Life Science Foundation, Mitsubishi Foundation, Suzuken Memorial Foundation, The Hori Science and Arts Foundation, Mochida Foundation, Takeda Science Foundation, Sakakibara Heart Foundation, Japan Heart Foundation, Nippon Shinyaku Co., Ltd., and Senshin Medical Research Foundation to Dr. Yura, the Japan Society for the Promotion of Science KAKENHI (grant 23K27594) to Dr. Takefuji, and the Japan Society for the Promotion of Science KAKENHI (grant 24K02444) to Dr. Murohara.

**Disclosures**

The authors declare no conflict of interest.

**Author contributions**

J. Yonekawa and Y. Yura conducted the majority of the experiments, acquired and analyzed the data, and wrote the manuscript. J. Luo, K. Kato, T. Hattori, R. Okamoto, M. Kizuki, E. Yura-Miura, K. Horitani, K.-

D. Min, and T. Emoto contributed to data acquisition and interpretation of experimental results. Y. Kawai, S. Ikeda, and H. Banno collected patient data. K. Walsh and M. Takefuji provided conceptual advice and overall study guidance. K. Walsh also provided the mice used in this study and revised the manuscript. Y. Yura, M. Takefuji, and T. Murohara provided research funding. T. Murohara supervised the project. All authors reviewed and approved the final manuscript.

## References


1. Kent KC. Clinical practice. Abdominal aortic aneurysms. N Engl J Med. 2014;371(22):2101–8.

2. Golledge J, et al. Lack of an effective drug therapy for abdominal aortic aneurysm. J Intern Med. 2020;288(1):6–22.

3. Nordon IM, et al. Pathophysiology and epidemiology of abdominal aortic aneurysms. Nat Rev Cardiol. 2011;8(2):92–102.

4. King SJ, et al. Heart Disease Mortality in the United States, 1970 to 2022. J Am Heart Assoc. 2025;14(13):38644.

5. Golledge J, et al. Pathogenesis and management of abdominal aortic aneurysm. Eur Heart J. 2023;44(29):2682–2697.

6. Wanhainen A, Mani K, Golledge J. Surrogate Markers of Abdominal Aortic Aneurysm Progression. Arterioscler Thromb Vasc Biol. 2016;36(2):236–244.

7. Quintana RA, Taylor WR. Cellular mechanisms of aortic aneurysm formation. Circ Res. 2019;124(4):607–618.

8. Dale MA, Ruhlman MK, Baxter BT. Inflammatory cell phenotypes in AAAs: their role and potential as targets for therapy. Arterioscler Thromb Vasc Biol. 2015;35(8):1746–1755.

9. Shimizu K, Mitchell RN, Libby P. Inflammation and cellular immune responses in abdominal aortic aneurysms. Arterioscler Thromb Vasc Biol. 2006;26(5):987–994.

10. Ladich E, et al. Vascular diseases: aortitis, aortic aneurysms, and vascular calcification. Cardiovasc Pathol. 2016;25(5):432–441.

11. Evans MA, Walsh K. Clonal hematopoiesis, somatic mosaicism, and age-associated disease. Physiol Rev. 2023;103(1):649–716.

12. Walsh K. The emergence of clonal hematopoiesis as a disease determinant. J Clin Invest. 2024;134(19). https://doi.org/10.1172/JCI180063.

13. Steensma DP, et al. Clonal hematopoiesis of indeterminate potential and its distinction from myelodysplastic syndromes. Blood. 2015;126(1):9–16.

14. Fuster JJ, Walsh K. Somatic Mutations and Clonal Hematopoiesis: Unexpected Potential New Drivers of Age-Related Cardiovascular Disease. Circ Res. 2018;122(3):523–532.

15. Yura Y, Sano S, Walsh K. Clonal Hematopoiesis: A New Step Linking Inflammation to Heart Failure. JACC Basic Transl Sci. 2020;5(2):196–207.

16. Wong WJ, et al. Clonal haematopoiesis and risk of chronic liver disease. Nature. 2023;616(7958):747–754.

17. Miller PG, et al. Association of clonal hematopoiesis with chronic obstructive pulmonary disease. Blood. 2022;139(3):357.

18. Kim PG, et al. Dnmt3a-mutated clonal hematopoiesis promotes osteoporosis. J Exp Med. 2021;218(12). https://doi.org/10.1084/JEM.20211872.

19. Daugherty A, Manning MW, Cassis LA. Angiotensin II promotes atherosclerotic lesions and aneurysms in apolipoprotein E-deficient mice. J Clin Invest. 2000;105(11):1605–1612.

20. Cochran JD, et al. Clonal Hematopoiesis in Clinical and Experimental Heart Failure With Preserved Ejection Fraction. Circulation. 2023;148(15):1165–1178.

21. Jaiswal S, et al. Age-related clonal hematopoiesis associated with adverse outcomes. N Engl J Med. 2014;371(26):2488–2498.

22. Kelly MJ, Igari K, Yamanouchi D. Osteoclast-Like Cells in Aneurysmal Disease Exhibit an Enhanced Proteolytic Phenotype. Int J Mol Sci. 2019;20(19). https://doi.org/10.3390/IJMS20194689.

23. Liu C, et al. Structural and functional insights of RANKL-RANK interaction and signaling. J Immunol. 2010;184(12):6910–6919.

24. Nakagawa N, et al. RANK is the essential signaling receptor for osteoclast differentiation factor in osteoclastogenesis. Biochem Biophys Res Commun. 1998;253(2):395–400.

25. Yamamoto M, et al. TNF receptor-associated factor 6 (TRAF6) plays crucial roles in multiple biological systems through polyubiquitination-mediated NF-κB activation. Proc Jpn Acad Ser B Phys Biol Sci. 2021;97(4):145–160.

26. Luckman SP, et al. Nitrogen-containing bisphosphonates inhibit the mevalonate pathway and prevent post-translational prenylation of GTP-binding proteins, including Ras. J Bone Miner Res. 1998;13(4):581–589.

27. Lacey DL, et al. Osteoprotegerin Ligand Is a Cytokine that Regulates Osteoclast Differentiation and Activation. Cell. 1998;93(2):165–176.

28. Wang W, et al. The Interaction between Lymphoid Tissue Inducer-Like Cells and T Cells in the Mesenteric Lymph Node Restrains Intestinal Humoral Immunity. Cell Rep. 2020;32(3). https://doi.org/10.1016/j.celrep.2020.107936.

29. Fuster JJ, et al. Clonal hematopoiesis associated with TET2 deficiency accelerates atherosclerosis development in mice. Science. 2017;355(6327):842–847.

30. Sano S, et al. Tet2-Mediated Clonal Hematopoiesis Accelerates Heart Failure Through a Mechanism Involving the IL-1β/NLRP3 Inflammasome. J Am Coll Cardiol. 2018;71(8):875–886.

31. Polizio AH, et al. Experimental TET2 Clonal Hematopoiesis Predisposes to Renal Hypertension Through an Inflammasome-Mediated Mechanism. Circ Res. 2024;135(9):933–950.

32. Zhang Q, et al. Tet2 is required to resolve inflammation by recruiting Hdac2 to specifically repress IL-6. Nature. 2015;525(7569):389–393.

33. Cull AH, et al. Tet2 restrains inflammatory gene expression in macrophages. Exp Hematol. 2017;55:56-70.e13.

34. Duplomb L, et al. Interleukin-6 inhibits receptor activator of nuclear factor kappaB ligand-induced osteoclastogenesis by diverting cells into the macrophage lineage: key role of Serine727 phosphorylation of signal transducer and activator of transcription 3. Endocrinology. 2008;149(7):3688–3697.

35. Zhou P, Zheng T, Zhao B. Cytokine-mediated immunomodulation of osteoclastogenesis. Bone. 2022;164. https://doi.org/10.1016/J.BONE.2022.116540.

36. Longo GM, et al. Matrix metalloproteinases 2 and 9 work in concert to produce aortic aneurysms. J Clin Invest. 2002;110(5):625–632.

37. Thompson RW, et al. Production and localization of 92-kilodalton gelatinase in abdominal aortic aneurysms. An elastolytic metalloproteinase expressed by aneurysm-infiltrating macrophages. J Clin Invest. 1995;96(1):318–326.

38. Jones GT, et al. Meta-Analysis of Genome-Wide Association Studies for Abdominal Aortic Aneurysm Identifies Four New Disease-Specific Risk Loci. Circ Res. 2017;120(2):341–353.

39. Auton A, et al. A global reference for human genetic variation. Nature. 2015;526(7571):68–74.

40. Pich O, et al. Discovering the drivers of clonal hematopoiesis. Nat Commun. 2022;13(1):1–12.

41. Yura Y, et al. The Cancer Therapy-Related Clonal Hematopoiesis Driver Gene Ppm1d Promotes Inflammation and Non-Ischemic Heart Failure in Mice. Circ Res. 2021;129(6):684–698.

42. Trachet B, et al. Performance Comparison of Ultrasound-Based Methods to Assess Aortic Diameter and Stiffness in Normal and Aneurysmal Mice. PLoS One. 2015;10(5):e0129007.

**Abbreviations**

| | |
|---|---|
| **AAA** | Abdominal Aortic Aneurysm |
| **ACP5** | Acid phosphatase 5, tartrate resistant |
| **ALN** | Alendronate |
| **AngII** | Angiotensin II |
| **ApoE** | Apolipoprotein E |
| **ASXL1** | Additional sex combs like 1 |
| **ATM** | Ataxia telangiectasia mutated |
| **BMT** | Bone marrow transplantation |
| **CCR2** | C-C Motif Chemokine Receptor 2 |
| **CHK2** | checkpoint kinase 2 |
| **DNMT3A** | DNA methyltransferase 3A |
| **HSPC** | Hematopoietic stem and progenitor cell |
| **Indel** | Insertion–deletion |
| **M-CSF** | Macrophage colony stimulating factor |
| **MMP** | Matrix metalloproteinase |
| **PPM1D** | protein phosphatase $Mg^{2+}/Mn^{2+}$ dependent 1D |
| **RANK** | Receptor activator of nuclear factor κB |
| **RANKL** | Receptor activator of nuclear factor κB ligand |
| **SCF-1** | Stem cell factor-1 |
| **SF3B1** | splicing factor 3b subunit 1 |
| **SRSF2** | serine and arginine rich splicing factor 2 |
| **sgRNA** | Single-guide RNA |
| **TagRFP** | Tag red fluorescent protein |
| **TET2** | Ten-eleven translocation-2 |
| **TP53** | tumor protein p53 |

| | | |
|---|---|---|
| 1 | **TRAP** | Tartrate-resistant acid phosphatase type 5 |
| 2 | **VAF** | Variant allele frequency |
| 3 | **WT** | Wild-type |
| 4 | | |

**Fig.1**

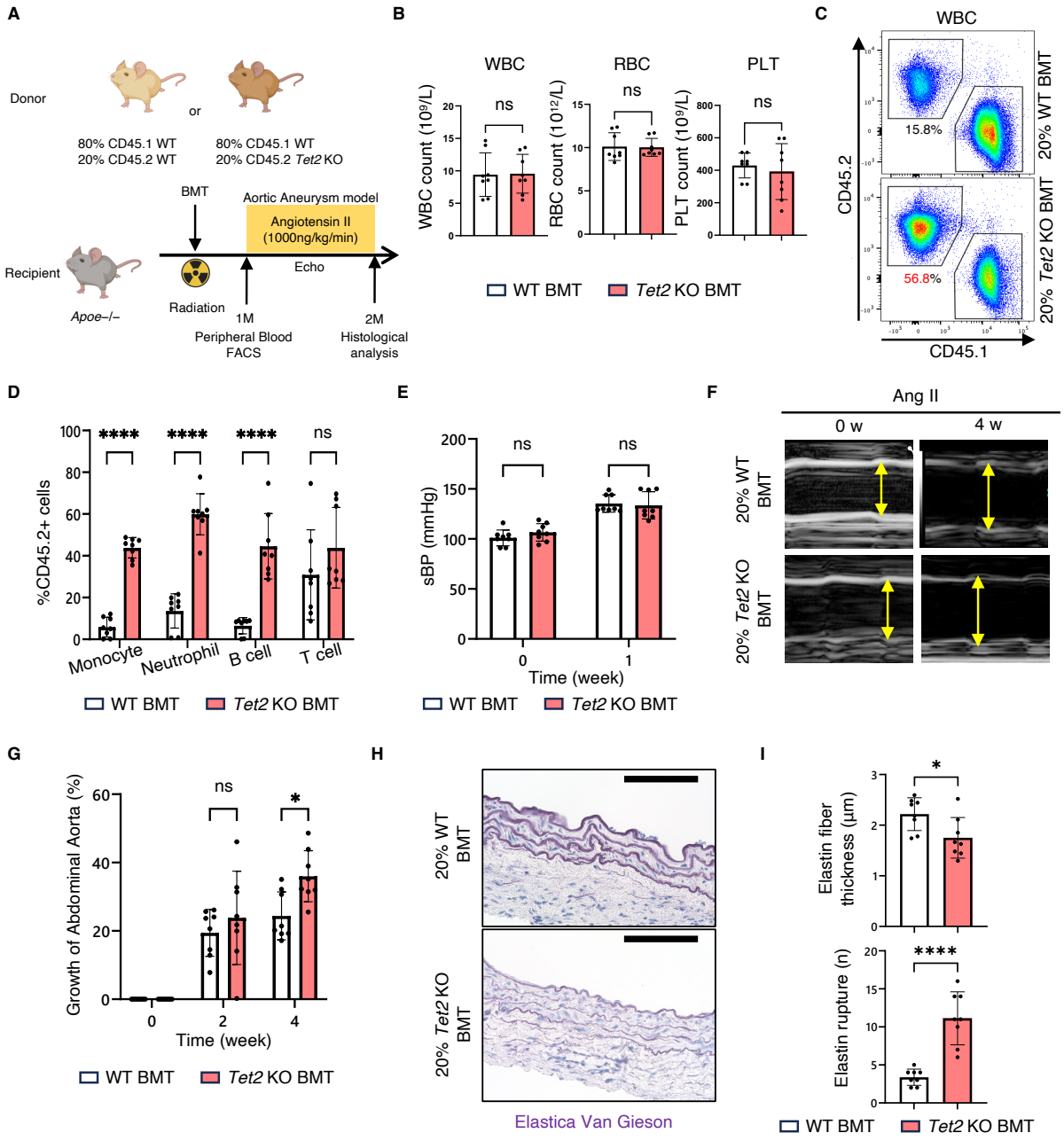


**Fig. 1. clonal hematopoietic mouse model shows greater aortic aneurysm formation in response to angiotensinII (AngII) infusion. (A)** Schematic of abdominal aortic aneurysm model establishment using Apolipoprotein E (*Apoe*)-KO mice and AngII infusion. To model clonal hematopoiesis, recipient mice received 80% Wild-type (WT) and 20% *Tet2*-KO bone marrow (BM) cells after

irradiation. Control mice received 100% WT BM. **(B)** The absolute number of white blood cells (WBCs), red blood cells (RBCs), and platelets (PLTs) in both experimental groups (n = 8 per genotype). Statistical significance was evaluated using unpaired two-tailed Welch's t test. **(C)** Representative flow cytometry gating plots of peripheral blood 4 weeks post-transplantation (n = 8 mice per genotype). **(D)** Quantification of peripheral blood populations 4 weeks post-transplantation (n = 8 mice per genotype). Statistical significance was evaluated using Mann-Whitney U test. **(E)** Systolic blood pressure measured using tail cuff plethysmography after 1 week of AngII infusion (n = 8 mice per genotype). Statistical significance was evaluated using two-way repeated ANOVA with Sidak multiple comparison test. **(F)** Representative ultrasound images of the abdominal aorta at 0 (baseline) and 4 weeks post-AngII infusion. Images are representative of n = 8 mice per genotype. **(G)** Quantification of abdominal aortic diameter at 0 (baseline), 2, and 4 weeks post-AngII infusion (n = 8 mice per genotype). Statistical significance was evaluated using two-way repeated ANOVA with Sidak multiple- comparison test. **(H)** Representative images of Elastica van Gieson staining of abdominal aorta tissue (scale bar = 100 μm). **(I)** Elastin fiber thickness and rupture counts in **H** (*n* = 8 mice per genotype). Statistical significance for elastin fiber thickness was evaluated using a two-tailed unpaired Student's t-test, and for rupture counts using a two-tailed Mann–Whitney U test. *P < 0.05; ****P < 0.0001.

Fig.2

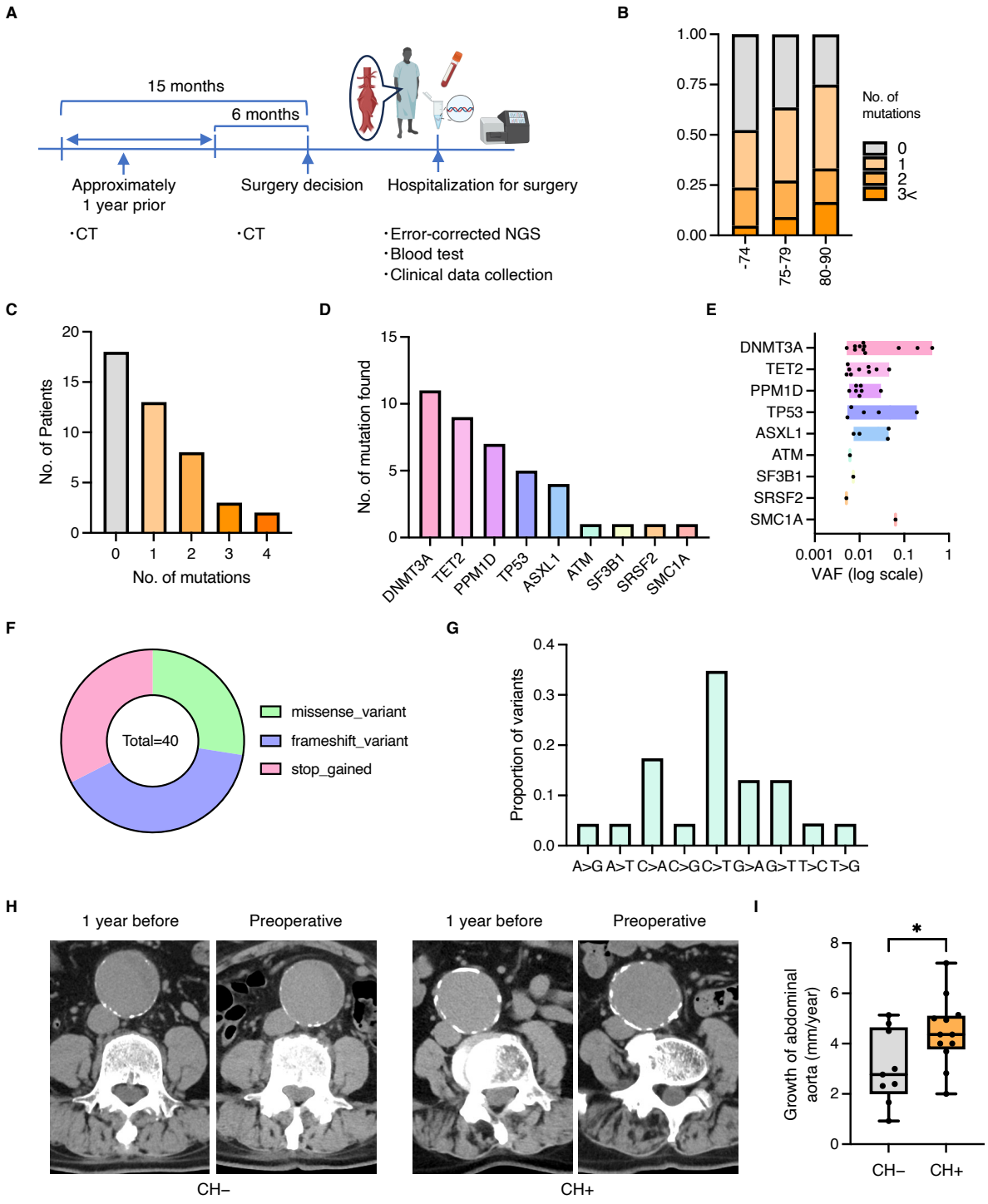


1 **Fig.2. Analysis of clonal hematopoiesis in patients with aortic aneurysm. (A)** Schematic overview

2 of the clinical follow-up protocol. **(B)** Age-stratified prevalence of the number of mutations per

individual. **(C)** Proportion of patients with specified number of clonal hematopoiesis mutations (n = 44). **(D)** Abundance of specified driver gene mutation in patient cohort (n = 40). **(E)** VAF distribution of driver genes (n = 40). The x-axis is shown on a logarithmic scale. **(F)** Proportions of different types of gene mutations (n = 40). **(G)** Proportions of different nucleotide substitutions (n = 24). **(H)** Representative CT images of aortic aneurysms with and without clonal hematopoiesis. Images are representative of 12 patients with clonal hematopoiesis and 9 patients without clonal hematopoiesis. **(I)** Aortic expansion rate in patients with clonal hematopoiesis (n = 12) and those without (n = 9). Data are presented as mean ± SEM. Statistical significance was determined by unpaired two-tailed Welch's t test ($p = 0.036$).

**Fig.3**

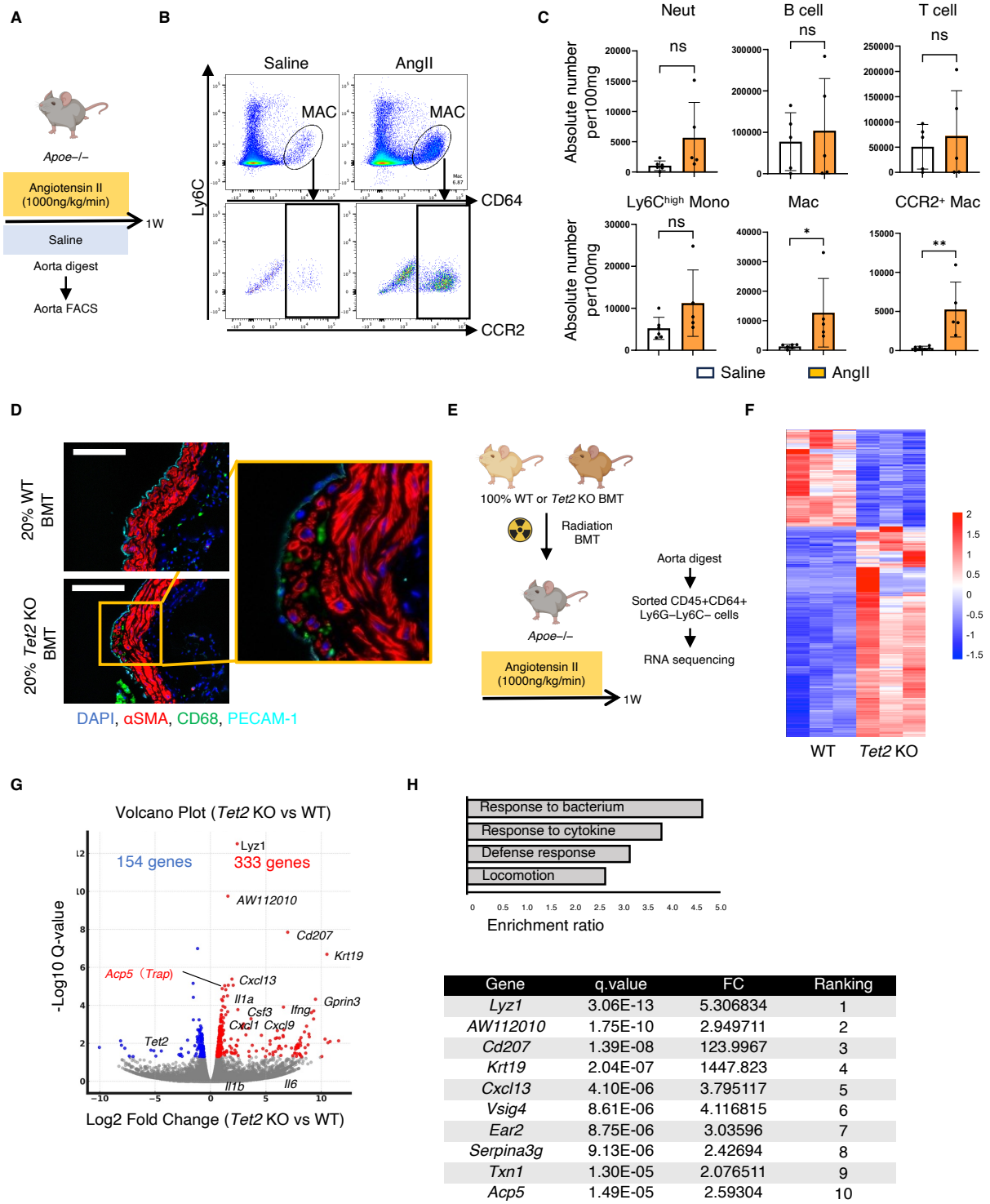


| Gene | q.value | FC | Ranking |
|---|---|---|---|
| *Lyz1* | 3.06E-13 | 5.306834 | 1 |
| *AW112010* | 1.75E-10 | 2.949711 | 2 |
| *Cd207* | 1.39E-08 | 123.9967 | 3 |
| *Krt19* | 2.04E-07 | 1447.823 | 4 |
| *Cxcl13* | 4.10E-06 | 3.795117 | 5 |
| *Vsig4* | 8.61E-06 | 4.116815 | 6 |
| *Ear2* | 8.75E-06 | 3.03596 | 7 |
| *Serpina3g* | 9.13E-06 | 2.42694 | 8 |
| *Txn1* | 1.30E-05 | 2.076511 | 9 |
| *Acp5* | 1.49E-05 | 2.59304 | 10 |

**Fig.3 (continued)**

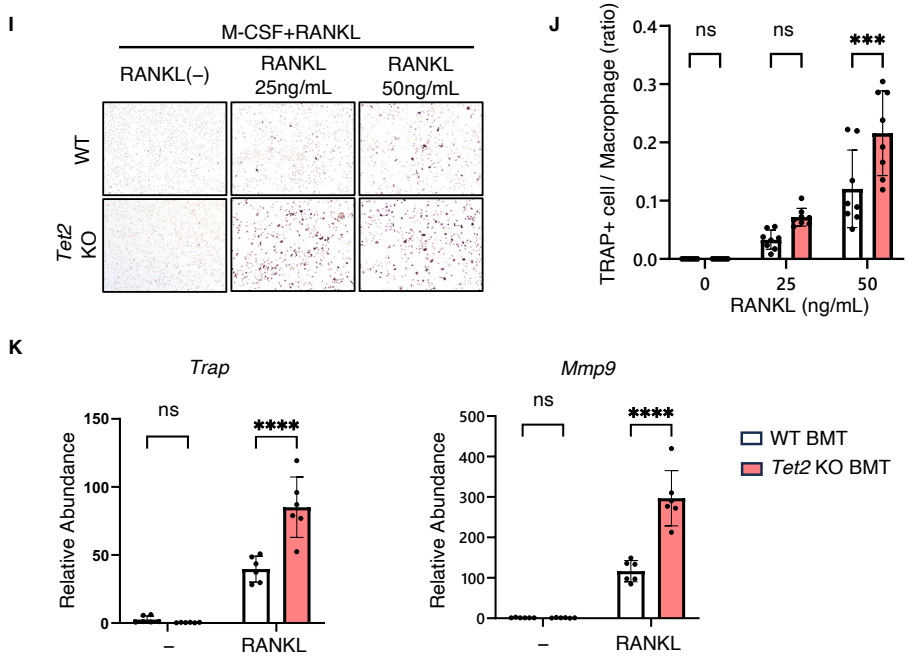


**Fig. 3. Bone marrow-derived macrophage involvement in experimental aortic aneurysm. (A)** Schematic of flow cytometry analysis and quantification of immune cells in abdominal aortic tissue from the abdominal aortic aneurysm model after 1 week of AngiotensinII (AngII) infusion. **(B)** Representative flow cytometry plots of digested abdominal aortic tissue 1 week post-AngII infusion (n = 5 mice per group). **(C)** Quantification of immune cell population in digested abdominal aortic tissue (absolute number per 100 mg). Neutrophils (Neut), Ly6C high monocytes (Ly6C$^{high}$ Mono), macrophages (Mac), and CCR2+ macrophages (CCR2+ Mac): saline n = 6, AngII n = 5; B cells (B cell) and T cells (T cell): n = 5 per group. Statistical significance was evaluated using Mann-Whitney U tests. **(D)** Representative images of CD68, α-smooth muscle actin (α-SMA), CD31/platelet endothelial cell adhesion molecule-1 (PECAM-1) and DAPI immunofluorescence staining of abdominal aortic tissue from aorta of control and 20% *Tet2*-KO bone marrow recipient mice after 1 week of AngII infusion (scale bar = 100 μm). Images are representative of n = 8 mice per genotype. **(E-H)** Schematic of RNA sequencing analysis of sorted macrophages from abdominal aorta of 100%

*Tet2*-KO bone marrow recipient mice after 1 week of AngII infusion. Upregulated and downregulated genes are presented as a heatmap and volcano plot. Gene Ontology (GO) enrichment analysis of upregulated genes in *Tet2*-deficient macrophages. The table lists the predominant genes ranked by q-value among significantly enriched pathways. **(I, J)** In vitro differentiation of bone marrow-derived macrophages. Representative images and quantification of the Tartrate-resistant acid phosphatase type 5-positive cell-to-macrophage ratio after receptor activator of nuclear factor κB ligand (RANKL) stimulation from 8 independent biological replicates per genotype. Statistical significance was evaluated using Mann-Whitney *U* test. **(K)** qPCR analysis of bone marrow-derived macrophages at 6 h after stimulation with 10 ng/mL lipopolysaccharide from 6 independent biological replicates per genotype. Statistical significance was evaluated using Mann-Whitney *U* test. *P < 0.05; **P < 0.01; ***P < 0.001; ****P < 0.0001.

Fig.4

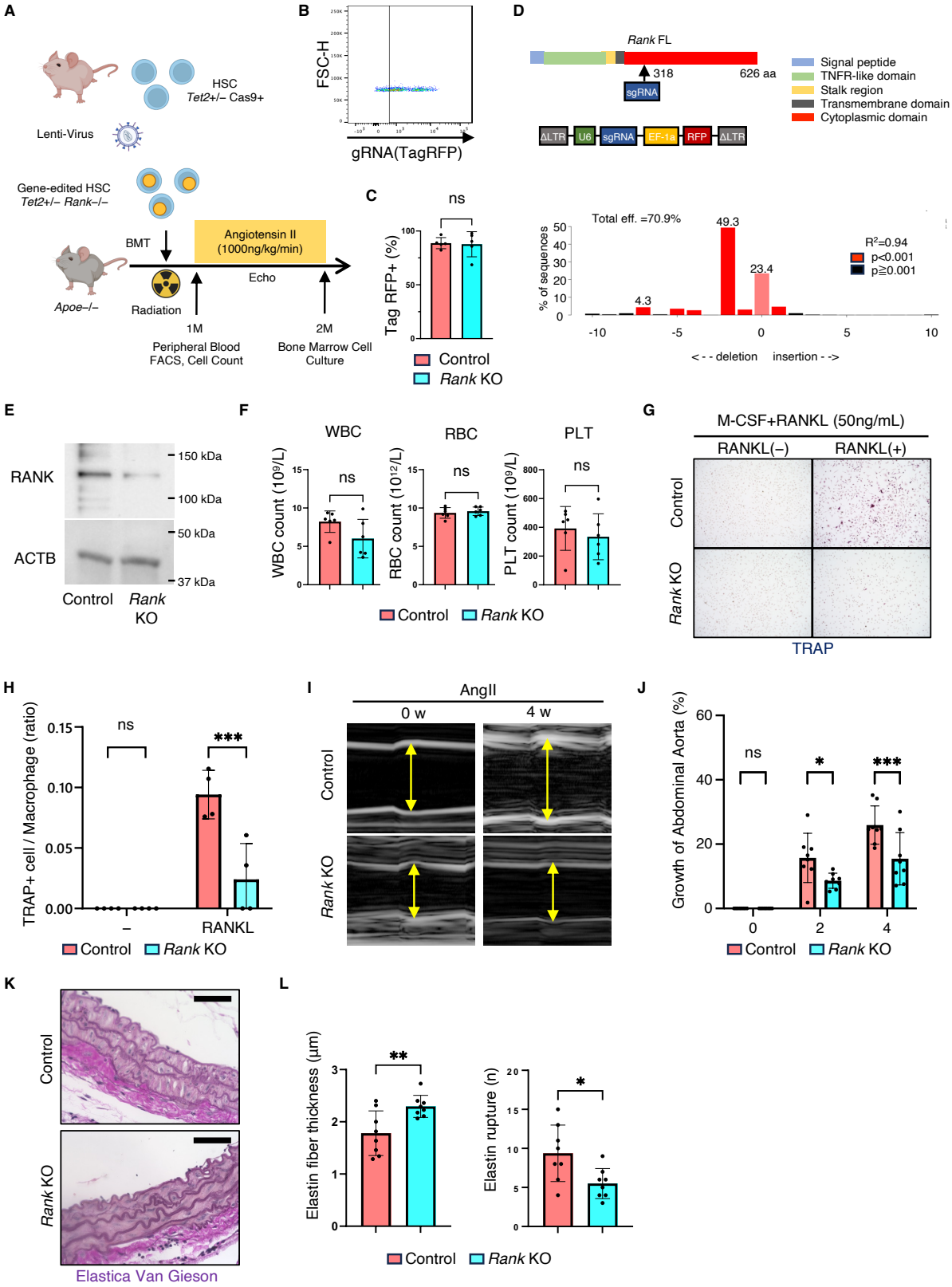


1 **Fig. 4. Receptor activator of nuclear factor κB (RANK)-RANK Ligand (RANKL) pathway has**

**critical role in Tartrate-resistant acid phosphatase type 5 (TRAP)-positive macrophage differentiation and abdominal aortic aneurysm disease progression in mice with clonal hematopoiesis.** **(A)** Schematic of *Tet2*/*Rank* double-KO model. Bone marrow-derived lineage-negative cells from Cas9-expressing *Tet2*$^{+/-}$ mice were transduced with lentivirus particles expressing single-guide RNA (sgRNA)/TagRFP and delivered to lethally irradiated Apolipoprotein E (*Apoe*)-KO mice. One month after bone marrow transplantation (BMT), peripheral blood was collected for flow cytometric analysis. **(B)** Expression of sgRNA/TagRFP vector at 4 weeks post-BMT in CD45+ cells. **(C)** Quantitative analysis of TagRFP-positive expression in cell populations derived from hematopoietic stem and progenitor cells transduced with lentiviral vectors encoding control or Rank-targeting sgRNA ($n$ = 5 mice per genotype). Statistical significance was evaluated using Mann-Whitney $U$ test. **(D)** Tracking of indels by decomposition analysis of the TagRFP-positive peripheral blood cells revealing insertions and deletions. **(E)** Immunoblot analysis of RANK expression in bone marrow-derived macrophages. Anti-RANK antibody detected multiple immunoreactive bands; the ~100-150 kDa band (putative modified form of RANK) is shown for KO validation. **(F)** Absolute number of WBCs, RBCs, and PLTs in both experimental groups ($n$ = 6 mice per genotype). Statistical significance was evaluated using unpaired two-tailed Welch's t-test. **(G, H)** In vitro differentiation of bone marrow-derived macrophages. Representative images and quantification of the TRAP-positive cell-to-macrophage ratio after RANKL stimulation from 4 independent biological replicates per genotype. Statistical significance was evaluated using Mann-Whitney $U$ test. **(I)** Representative ultrasound images of the abdominal aorta at 0 (baseline) and 4 weeks post-AngII infusion (n = 8 mice per genotype). **(J)** Quantification of abdominal aortic diameter at 0 (baseline), 2, and after 4 weeks of Angiotensin II (AngII) infusion in control and RANK KO mice (n = 8 mice per genotype). Statistical significance was evaluated using two-way repeated ANOVA with Sidak multiple- comparison test. **(K)** Representative images of Elastica van Gieson staining of abdominal aorta tissue (scale bar = 100 μm). **(L)** Elastin fiber thickness and rupture counts in **J** ($n$ = 8 mice per genotype). Statistical significance for elastin fiber thickness was evaluated using a two-tailed unpaired Student's t-test, and for rupture counts using a two-tailed Mann–Whitney U test. *P < 0.05; **P < 0.01; ***P < 0.001.

Fig.5

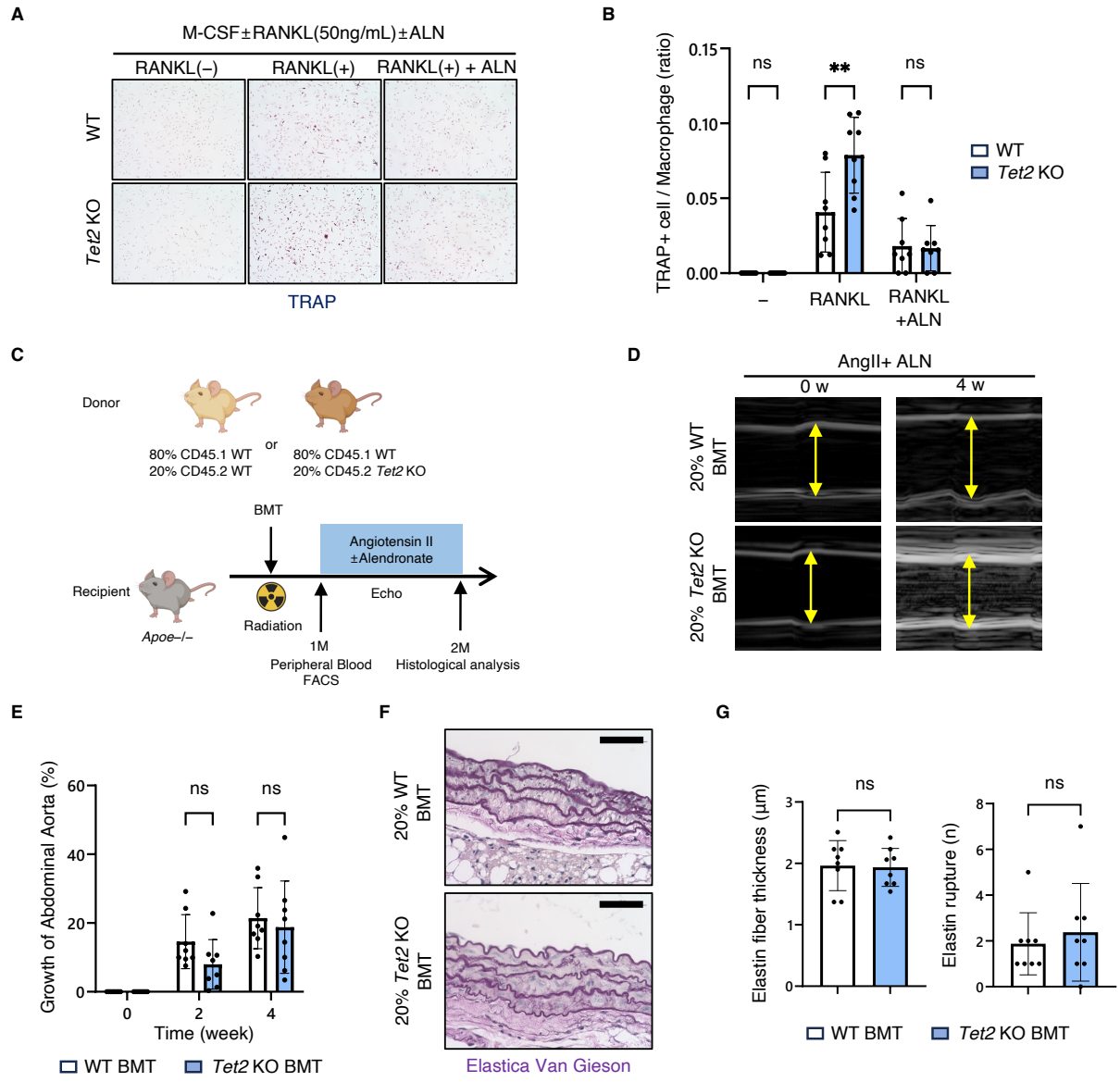


**Fig.5. Pharmacological inhibition of tartrate-resistant acid phosphatase type 5 (TRAP)-positive macrophage ameliorates abdominal aortic aneurysm phenotype in mice with Tet2 clonal hematopoiesis. (A, B)** In vitro differentiation of bone marrow-derived macrophages. Representative images and quantification of the TRAP-positive cell-to-macrophage ratio after receptor activator of nuclear factor κB ligand (RANKL) stimulation, with or without alendronate (ALN) treatment from 8 independent biological replicates per genotype. Statistical significance was evaluated using Mann-Whitney *U* test. **(C)**

Schematic of in vivo experimental design using clonal hematopoiesis and abdominal aortic aneurysm model with additional ALN treatment. **(D)** Representative ultrasound images of the abdominal aorta at 0 (baseline) and 4 weeks post- angiotensin II(AngII) infusion (n = 8 mice per genotype). **(E)** Quantification of abdominal aortic diameter at 0 (baseline), 2, and 4 weeks post-AngII infusion with ALN treatment (n = 8 mice per genotype). Statistical significance was evaluated using two-way repeated ANOVA with Sidak multiple- comparison test. **(F, G)** Representative images of Elastica van Gieson staining of abdominal aortic tissue and quantification of elastin fiber thickness and elastin rupture (*n* = 8 mice per genotype) (Scale bar = 100 μm). Statistical significance for elastin fiber thickness was evaluated using a two-tailed unpaired Student's t-test, and for rupture counts using a two-tailed Mann–Whitney U test. *P < 0.05; **P < 0.01; ***P < 0.001; ****P < 0.0001.

**Fig.6**

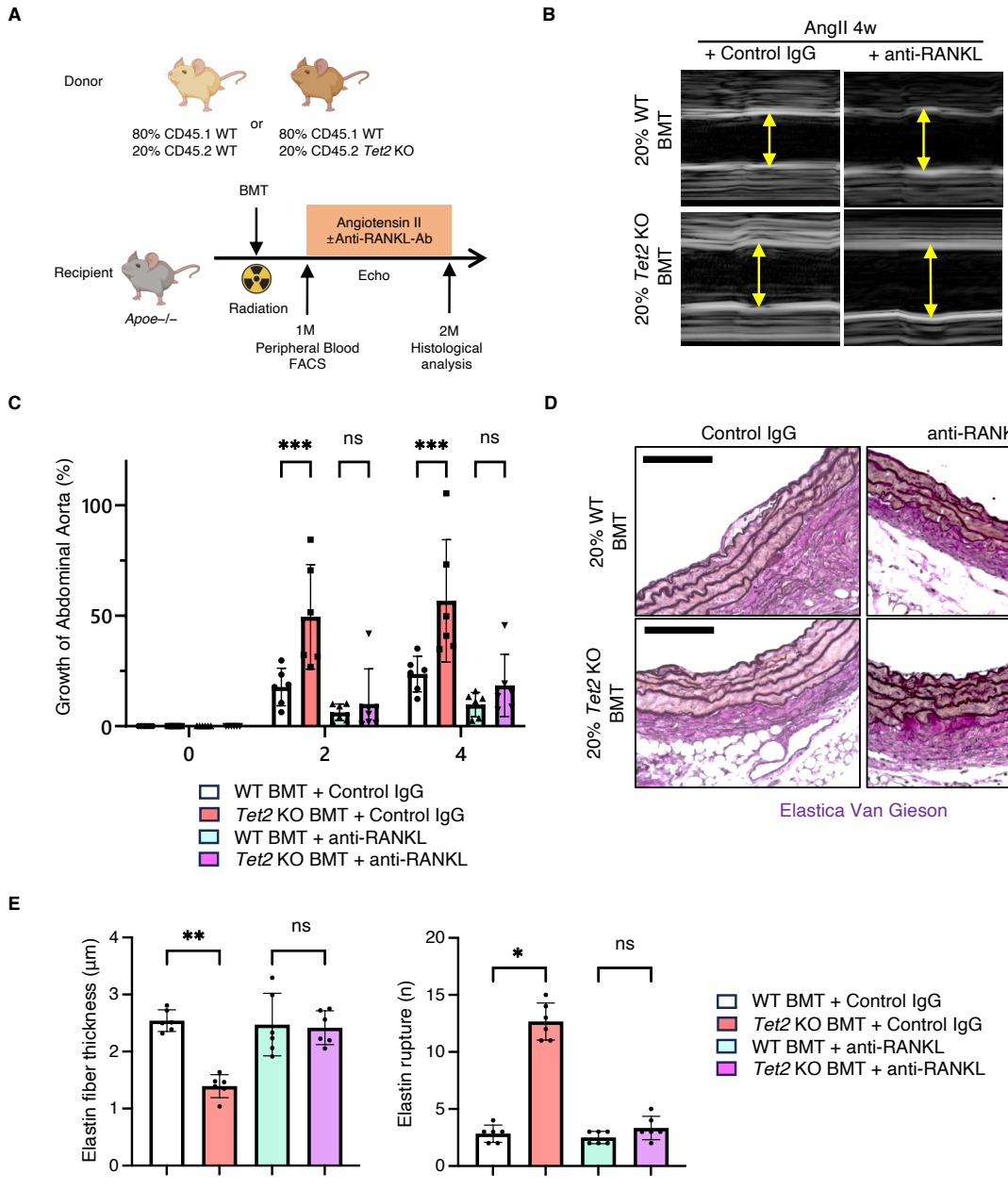


**Fig.6 Pharmacological inhibition of tartrate-resistant acid phosphatase type 5 (TRAP)-positive macrophage by anti-receptor activator of nuclear factor κB Ligand (RANKL) antibody ameliorates abdominal aortic aneurysm (AAA) phenotype in mice with clonal hematopoiesis. (A)** Schematic of in vivo experimental design using clonal hematopoiesis and abdominal aortic aneurysm model with Anti-RANKL antibody treatment. **(B)** Representative ultrasound images of the abdominal aorta at 4 weeks post-

Angiotensin II (AngII) infusion (n = 6 mice per group). **(C)** Quantification of abdominal aortic diameter at 0 (baseline), 2, and 4 weeks post-AngII infusion with Anti-RANKL antibody treatment (n = 6 mice per group). Statistical significance was evaluated using two-way repeated ANOVA with Sidak multiple-comparison test. **(D, E)** Representative images of Elastica van Gieson staining of abdominal aortic tissue and quantification of elastin fiber thickness and elastin rupture (*n* = 6 mice per group) (scale bar = 100 μm). Statistical significance was evaluated using the Kruskal–Wallis test followed by Dunn's multiple comparison test. Selected pairwise comparisons are shown for clarity. *P < 0.05; **P < 0.01; ***P < 0.001.

**Graphical abstract**

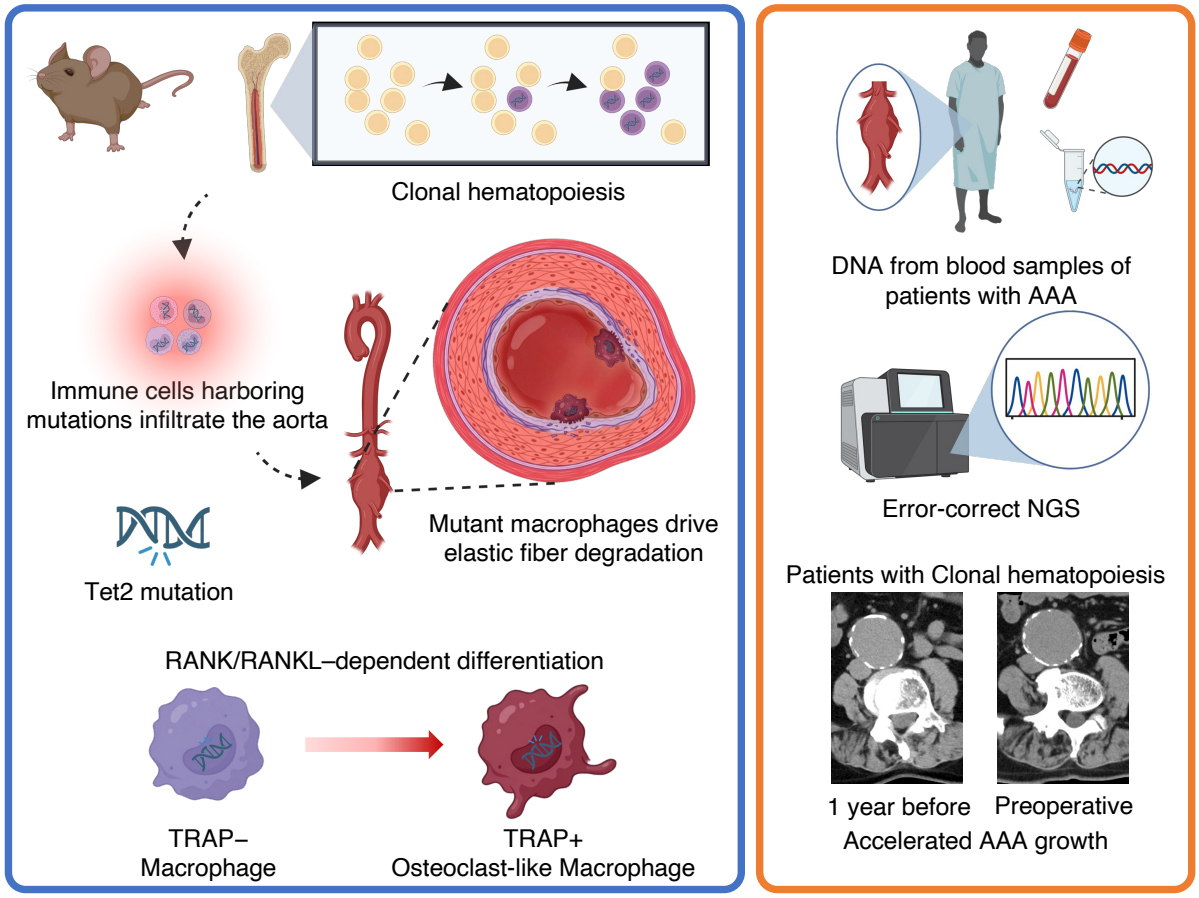


1

2

| | CH (-) (n=16) | CH (+) (n=28) | P-value |
|---|---|---|---|
| Age (years) | 73.4 ± 9.5 | 75.8 ± 6.5 | 0.332 |
| Body height (m) | 1.66 ± 0.07 | 1.65 ± 0.07 | 0.588 |
| Body weight (kg) | 63.3 ± 9.3 | 64.4 ± 11.4 | 0.765 |
| Body mass index (kg/m$^2$) | 22.9 ± 3.1 | 23.5 ± 3.6 | 0.553 |
| eGFR (mL/min/1.73m$^2$) | 53.1 ± 15.8 | 55.9 ± 17.9 | 0.837 |
| Sex (Male) | 15 (93.7%) | 25 (89.3%) | 0.630 |
| Hypertension | 11 (68.8%) | 23 (82.1%) | 0.319 |
| Diabetes | 2 (12.5%) | 9 (32.1%) | 0.155 |
| Dyslipidemia | 11 (68.8%) | 26 (92.9%) | 0.101 |
| Coronary Artery Disease | 6 (37.5%) | 12 (46.4%) | 0.576 |
| Heart Failure | 3 (18.8%) | 6 (21.4%) | 0.837 |
| Smoking, never | 2 (16.7%)[A] | 5 (22.7%)[A] | 0.687 |
| Smoking, former | 3 (25%)[A] | 10 (45.5%)[A] | 0.254 |
| Smoking, current | 7 (58.3%)[A] | 7 (31.8%)[A] | 0.142 |
| Family History | 0 | 3 (10.7%) | 0.213 |
| Diameter of Abdominal Aorta (mm) | 55.9 ± 9.3 | 53 ± 7.8 | 0.280 |

eGFR, estimated glomerular filtration rate.

[A]The value was available in 12 subjects of CH (-) and 22 patients with CH (+).

**Table 1. Clinical Characteristics of Patients with abdominal aortic aneurysm with and without Clonal Hematopoiesis.** Continuous variables are expressed as mean (standard deviation), and categorical variables are expressed as frequencies.

| | CH (-) (n=9) | CH (+) (n=12) | P-value |
|---|---|---|---|
| Age (years) | 75.4 ± 9.2 | 73.5 ± 4.6 | 0.530 |
| Body height (m) | 1.66 ± 0.06 | 1.64 ± 0.07 | 0.516 |
| Body weight (kg) | 62.9 ± 10.5 | 68.5 ± 10.8 | 0.254 |
| Body mass index (kg/m$^2$) | 22.9 ± 3.7 | 25.4 ± 3.2 | 0.113 |
| eGFR (mL/min/1.73m$^2$) | 49.0 ± 12.8 | 63.0 ± 18.4 | 0.066 |
| Sex (Male) | 9 (100%) | 10 (83.3%) | 0.217 |
| Hypertension | 7 (77.8%) | 10 (83.3%) | 0.400 |
| Diabetes | 1 (11.1%) | 4 (33.3%) | 0.259 |
| Dyslipidemia | 7 (77.8%) | 12 (100%) | 0.094 |
| Coronary Artery Disease | 5 (55.6%) | 5 (41.7%) | 0.552 |
| Heart Failure | 3 (33.3%) | 1 (8.3%) | 0.164 |
| Smoking, never | 2 (22.2%) | 3 (25%) | 0.793 |
| Smoking, former | 2 (22.2%) | 5 (41.7%) | 0.375 |
| Smoking, current | 5 (55.6%) | 4 (33.3%) | 0.552 |
| Family History | 0 | 2 (16.7%) | 0.217 |
| Diameter of Abdominal Aorta (mm) | 53.2 ± 4.8 | 53.5 ± 7.6 | 0.925 |
| Abdominal Aortic Diameter follow-up period (months) | 11.4±2.6 | 11.3±2.7 | 0.870 |
| Growth of Abdominal Aorta (mm/year) | 2.8±1.3 | 4.3±2.8 | 0.036 |

eGFR, estimated glomerular filtration rate.

**Table 2. Clinical Characteristics of Patients with abdominal aortic aneurysm with and without Clonal Hematopoiesis and longitudinal imaging for aneurysm growth rate.** Continuous variables are expressed as mean (standard deviation), and categorical variables are expressed as frequencies.